Cell Death and Differentiation (2017) 24, 225–237
 1350-9047/17

www.nature.com/cdd

Hedgehog signaling in bone regulates whole-body energy metabolism through a bone–adipose endocrine relay mediated by PTHrP and adiponectin

Xu Zhang[1], Qianni Cheng[2], Yixiang Wang[3], Po Sing Leung[2] and Kinglun Kingston Mak*[,1,4,5]

Bone plays a role in energy metabolism, but the interplay between bone and other organs in this process is not completely understood. Here, we show that upregulated Hh signaling in bones results in increased whole-body energy expenditure, white adipose tissue (WAT) browning, hypoglycemia and skeletal muscle atrophy. We found that Hh signaling induces PTHrP secretion from bones and causes WAT browning. Injection of PTHrP-neutralizing antibody attenuates WAT browning and improves the circulating blood glucose level while high-fat diet treatment only rescues hypoglycemia. Furthermore, bone-derived PTHrP stimulates adiponectin secretion in WAT and results in systemic increase of fatty acid oxidation and glucose uptake. Mechanistically, PTHrP activates both PKA/cAMP and Akt/Foxo pathways for Ucp1 expression in WAT. PTHrP couples adiponectin actions to activate the AMPK pathway in the skeletal muscles and liver, respectively, for fatty acid oxidation. Our findings establish a new bone–adipose hormonal relay that regulates whole-body energy metabolism.
Cell Death and Differentiation (2017) **24,** 225–237; doi:10.1038/cdd.2016.113; published online 14 October 2016

Type 2 diabetes mellitus, obesity and osteoporosis are major public health problems worldwide, and the rate of people suffering with these conditions increases exponentially every year.[1,2] In the past, these conditions have been viewed as separate diseases. However, accumulating evidence indicates that these conditions share similar pathophysiological mechanisms and the concept of bone and adipose tissues as inert metabolic tissues are recently being reevaluated.[3] Indeed, bone mineral density has been shown to be associated with obesity and glucose metabolism, respectively, in many previous studies,[4–7] but the correlation of bone phenotypes with obesity and diabetes remain controversial. Recently, bone has been proven molecularly to play an active role in the regulation of energy metabolism in the pancreas[8,9] and male fertility in testes.[10] These findings raise the important roles of the skeleton in systemic control of energy metabolism and physiology.

Osteocalcin, a protein specifically secreted by osteoblasts into circulation, has been demonstrated to serve as a bone-derived hormone in regulating bone and glucose metabolism as well as fat mass.[8,9] Further experiments suggest the existence of a bone–pancreas endocrine loop in which insulin signaling activates bone resorption with the secretion of undercarboxylated osteocalcin.[11,12] Yet, evidence from another study by Yoshikawa *et al.*[13] tested the hypothesis that fewer osteoblasts might mean reduce energy metabolism. The mice with osteoblast ablation had a significant reduction of insulin secretion and resulted in hyperglycemia, glucose intolerance and decreased insulin sensitivity. These effects are similar with the phenotypes observed in the osteocalcin-deficient mice. However, the osteoblast-ablated mice also showed a decrease in gonadal fat and increased energy expenditure, which are in contrast to the phenotypes of the osteocalcin-deficient mouse model. These data suggest that in addition to osteocalcin, osteoblasts secrete other energy metabolism-regulating hormones in metabolic control of fat tissues. Further investigation is necessary to determine the active roles of the bone in the regulation of fat mass and glucose metabolism.

Hedgehog (Hh) signaling plays important roles in endochondral bone formation and bone homeostasis. During embryonic development, Hh signaling activates the expression of parathyroid hormone-related protein (PTHrP) in articular chondrocytes to regulate the pace of chondrocyte hypertrophy in the developing growth plates.[14,15] It is also required for osteoblast differentiation by controlling the expression of *Runx2*.[14] However, during postnatal bone remodeling, Hh signaling plays bi-facet roles in controlling bone mass. Partial upregulation of Hh signaling by *Ptch1* haploinsufficeny increases bone mass,[16] whereas ubiquitous upregulation of Hh signaling specifically in mature osteoblasts promotes both bone formation and bone resorption.[17] The

[1]Ministry of Education Key Laboratories for Regenerative Medicine, School of Biomedical Sciences, Faculty of Medicine, Shatin, The Chinese University of Hong Kong, HKSAR, China; [2]Reproduction, Development and Endocrinology Thematic Research Program, School of Biomedical Sciences, The Chinese University of Hong Kong, Shatin, HKSAR; [3]Department of Imaging and Interventional Radiology, Faculty of Medicine, The Chinese University of Hong Kong, Shatin, HKSAR; [4]Stem Cell and Regeneration Thematic Research Program, School of Biomedical Sciences, The Chinese University of Hong Kong, Shatin, HKSAR and [5]School of Biomedical Sciences Core Laboratory, Shenzhen Research Institute, The Chinese University of Hong Kong, Shenzhen 518057, China

*Corresponding author: KK Mak, Stem Cell and Regeneration, School of Biomedical Sciences, The Chinese University of Hong Kong, Room 125A, Lo Kwee-Seong Integrated Biomedical Sciences Building, Area 39, Shatin, HKSAR. Tel: +852 3943 4497; Fax: +852 2603 5123; E-mail: kmak@cuhk.edu.hk

Abbreviations: PTHrP, parathyroid hormone-related protein; Hh, hedgehog; eWAT, epididymal white adipose tissue; iWAT, inguinal white adipose tissues; HFD, high-fat diet; ACC, acetyl-coA carboxylase; Ucp1, uncoupling protein-1

Received 26.5.16; revised 01.9.16; accepted 14.9.16; Edited by N Chandel; published online 14.10.16

non-cell autonomous activity of Hh signaling in osteoclast differentiation is mediated by the secretion of PTHrP from mature osteoblasts, which induces *Rankl* expression.[17] These data demonstrate that Hh signaling in bones have both cell-autonomous and non-cell-autonomous mechanisms to meticulously regulate bone remodeling. It remains to question whether the dynamic control of bone mass by Hh signaling affects whole-body energy metabolism through endocrine regulation.

Here, we investigated the role of Hedgehog signaling in bones for whole-body energy metabolism. Apart from previously reported bone phenotypes,[17] we found that upregulated Hh signaling in mature osteoblasts results in increased energy expenditure, white adipose tissues (WATs) browning, hypoglycemia and skeletal muscle atrophy. Importantly, these systemic effects are independent of osteocalcin or insulin secretion, and are initiated by bone-derived hormone PTHrP. In addition, we found that PTHrP stimulates adiponectin secretion in adipose tissues that contributes to systemic increase of fatty acid oxidation. Our results establish a new bone–adipose endocrine axis in regulating whole-body metabolism.

Results

Upregulated Hh signaling in mature osteoblasts increases systemic energy expenditure. We previously analyzed the functions of Hh signaling in bone remodeling by upregulated Hh signaling specifically in mature osteoblasts.[17] Apart from osteopenia phenotype being reported, the *Ptch1$^{c/c}$;HOC-Cre* mutant mice also displayed remarkable growth retardation (Figures 1a and b) and rapid breathing (Supplementary Movies S1 and S2). These observations led us to examine whether energy metabolism was perturbed in these mice. First, we examined metabolic parameters in the mutant mice using metabolic cages. The overall rate of oxygen consumption in the mutant mice was significantly higher (Figures 1c and e). Energy expenditure (heat) was increased in both diurnal and nocturnal periods (Figures 1d and f), despite reduced locomotor activity (Figure 1g). Food intake was also increased (Figure 1h). Taken together, our data indicate that systemic energy expenditure is increased when Hh signaling is upregulated specifically in bones.

Browning of WAT in the *Ptch1$^{c/c}$;HOC-Cre* mutant mice. To determine the cause of weight loss in our mutant mice, we performed whole-body composition analysis. Both adiposity and lean mass of the mutant mice were significantly lower than that of the control littermates (Figures 2a and b). NMR scanning also showed massive fat atrophy (Figure 2c). Furthermore, micro-CT analysis showed that both visceral fat and subcutaneous fat were significantly reduced in the mutant mice (Figures 2d–e). The tissue weight of epididymal fat (eWAT), a visceral fat depot, and inguinal adipose tissues (iWAT), a subcutaneous fat depot, were also reduced significantly (Figure 2f). Histological examination revealed significant smaller adipocytes with multilocular cytoplasm in both eWAT and iWAT (Figures 2g–k). The expression of Uncoupling protein-1 (Ucp1), a specific marker for adipose tissue browning, was significantly increased (Figures 3a–c). Furthermore, thermogenesis (*Ucp1, Cidea, Cox7a1, Pgc1a, Dio2, Prdm16*) and beige cell (*CD137, TMEM26* and *Tbx1*) marker gene expressions were all strongly upregulated in both eWAT and iWAT of the *Ptch1$^{c/c}$;HOC-Cre* mutant mice, respectively (Figures 3d and e). Genes involved in energy metabolism, including lipolytic enzymes, glucose transporters and *β*-oxidation (*Acox1, Acsl1, Atgl, Glut1* and *Hsl)* were also significantly increased (Figures 3f and g). Consistently, the serum triglyceride level was reduced (Figure 3h). In contrast to massive atrophy of WATs, interscapular brown adipose tissues (BAT) in the mutant mice were comparable in size to age-matched littermates, albeit the difference in overall body weight (Supplementary Figure S1a). The histology and size of brown adipocytes in the mutant mice were largely normal (Supplementary Figures S1b and c), but the expression of Ucp1 was greatly increased (Supplementary Figures S1d and e). In addition, gene expressions involved in thermogenesis and *β*-oxidation were also greatly induced in BAT (Supplementary Figure S1f). Altogether, our data indicate that upregulated Hh signaling in bone elicits WAT browning and enhances fatty acid oxidation in adipose tissues that results in increased energy expenditure.

Bone-derived PTHrP increases fatty acid oxidation of adipose tissues. The non-cell autonomous activity of Hh signaling in bones to induce metabolic changes in the *Ptch1$^{c/c}$;HOC-Cre* mutant mice prompted us to determine secretory factors produced in the osteoblasts that are regulated by Hh signaling. PTHrP is one of the top candidates because it is induced by Hh signaling in regulating bone remodeling. Bone tissues isolated from the *Ptch1$^{c/c}$;HOC-Cre* mutant mice and *Ptch1$^{c/c}$* primary osteoblasts infected with *Cre-adenovirus* both showed significant increase in *PTHrP* expression (Figures 4a and b). In addition, treatment with Hh agonist purmorphamine in wild-type primary osteoblasts also induced *PTHrP* expression in a dose- and time-dependent manner (Figure 4c). Thus, we investigated whether PTHrP is secreted into circulation by examining the serum level of PTHrP in the *Ptch1$^{c/c}$;HOC-Cre* mutant mice. As expected, the circulating PTHrP level was markedly increased as compared with that of the control littermates (Figure 4d). Next, we tested whether PTHrP signaling is activated in WAT by examining the expression of PTHrP receptor PTH1R in the adipose tissues. Both eWAT and iWAT isolated from the mutant mice displayed significant upregulation of *PTH1R* expression (Figure 4e) suggesting that bone-derived PTHrP is responsible for WAT browning. To further confirm our findings, we cultured preadiocyte cell line 3T3-L1 and differentiated them into mature adipocytes *in vitro* and treated these cells with recombinant PTHrP (Figure 4f). Key thermogenesis markers were all strongly upregulated by PTHrP treatment in a dose-dependent manner. To demonstrate that osteoblasts are the source of PTHrP secretion in the *Ptch1$^{c/c}$;HOC-Cre* mutant mice, we isolated bone chips from the long bones of the mice and cultured them *in vitro*. Conditioned medium was then collected for three consecutive days. When differentiated 3T3L1 cells were treated with the conditioned medium isolated from the mutant bones, all the thermogenesis markers were strongly induced (Figure 4g).

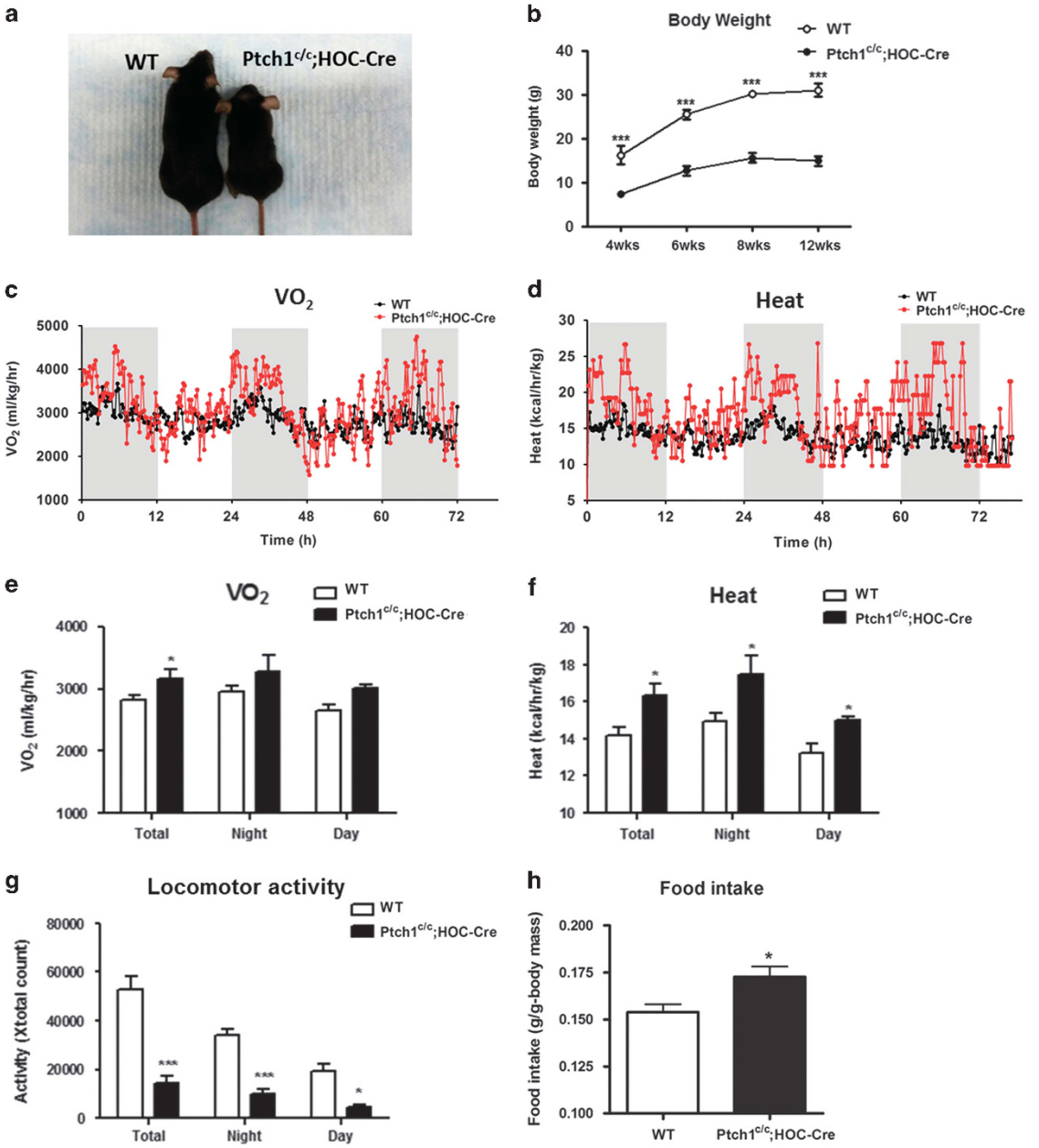

Figure 1 Metabolic phenotypes of the *Ptch1$^{c/c}$;HOC-Cre* mutant mice. (**a**) Representative image of the body size of the *Ptch1$^{c/c}$;HOC-Cre* mouse and wild-type (WT) littermate at 2 months old. (**b**) Body weight curve of wild type and *Ptch1$^{c/c}$;HOC-Cre* mice from 4 to 12 weeks ($n=6$ for each group). (**c** and **d**) Oxygen consumption (**c**) and heat output (**d**) measured every 10 min for 72 h. The gray column represents nocturnal period and the white column represents diurnal period. (**e** and **f**) Average values of oxygen consumption (**e**) and heat output (**f**) of mice as shown ($n=6$ for WT; $n=5$ for *Ptch1$^{c/c}$;HOC-Cre*). (**g**) Average locomotor activity measured for three consecutive days. (**h**) Average food intake per body weight measured for three consecutive days ($n=8$ for each group). Data are presented as mean ± S.E.M. (*$P<0.05$; ***$P<0.001$)

Furthermore, co-treatment with PTHrP-neutralizing antibodies in the conditioned medium ameliorated its effect. This result indicates that Hh signaling induces bone-derived PTHrP secretion that increases thermogenesis of WAT. We further examined this effect *in vivo* by injecting PTHrP-neutralizing antibodies into the *Ptch1$^{c/c}$;HOC-Cre* mutant mice. After four rounds of PTHrP-neutralizing antibodies injection, the body weight was significantly improved (Figure 4h). Both visceral and subcutaneous fat depots contributed to the weight gain but the increase was more obvious in visceral fat depots (Figures 4i and j). However, no obvious change of bone mass was observed in the mutant mice (Supplementary Figures S2e–g), suggesting that the body weight gain is mainly due to the increase of adipose tissues. PTHrP-neutralizing antibodies injection into wild-type mice also showed no obvious effects in adipose and bone tissues, respectively (Supplementary Figure S2). The expression profiles of all the energy metabolism markers induced in

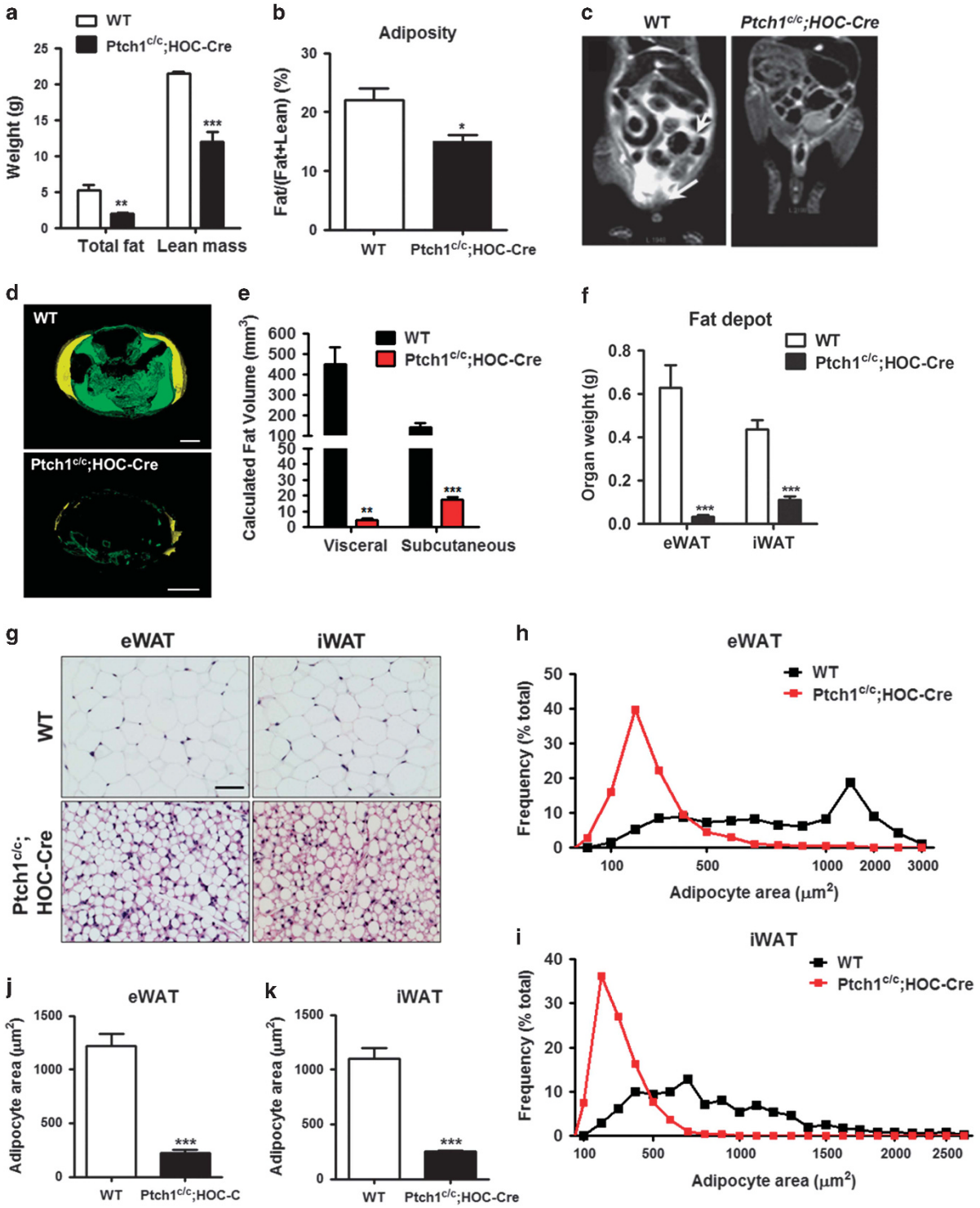

Figure 2 Reduced adiposity in the *Ptch1$^{c/c}$;HOC-Cre* mice. (**a**) Whole-body composition analysis of total fat and lean mass by weight ($n=5$ for each group at 2-month-old). (**b**) Adiposity as represented by (Fat/(Fat+Lean)%) of the mice with genotypes as shown. (**c**) Sagittal images of nuclear magnetic resonance (NMR) scan of 1-month-old mice as shown. White arrows pointed to visceral fat as shown by intense white color ($n=3$ for each genotype). (**d**) Cross images of μCT scan of lumbar column L1–L5 of 1.5-month-old mice as shown. Green represents visceral fat depots and yellow represents subcutaneous fat depots (scale bar = 5 mm, $n=3$ for each genotype). (**e**) Quantification of fat depots as shown in (**d**). (**f**) Fat tissue weight of epididymal white adipose tissue (eWAT) and inguinal white adipose tissue (iWAT) in mice with genotype as shown ($n=4$ for each genotype). (**g**) Representative images of hematoxylin and eosin (h&e) staining of eWAT and iWAT (scale bar = 50 μm, $n=3$ for each genotype). (**h** and **i**) Profiles of adipocyte size distribution of eWAT (**h**) and iWAT (**i**) as shown in (**g**). (**j** and **k**). Quantification of average adipocyte size of eWAT (**j**) and iWAT (**k**) as shown in (**g**). Data are presented as mean ± S.E.M. (*$P<0.05$; **$P<0.01$; ***$P<0.001$)

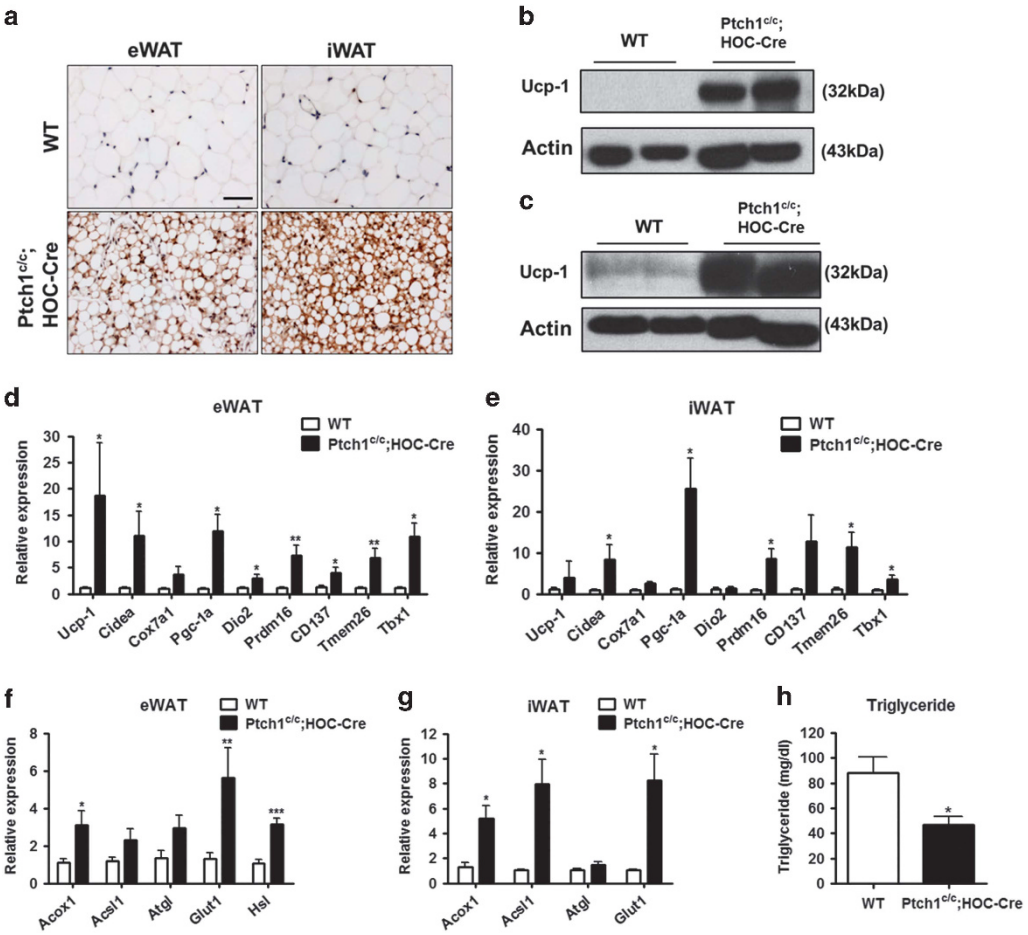

Figure 3 Enhanced thermogenesis and WAT browning in the *Ptch1$^{c/c}$;HOC-Cre* mice. (**a**) Immunostaining of Ucp1 expression in the eWAT and iWAT tissues of the mice with genotypes as shown (scale bar = 50 μm, $n = 3$ for each genotype). (**b** and **c**) Immunoblots of Ucp1 expression in the eWAT (**b**) and iWAT tissues (**c**) ($n = 4$ for each genotype). (**d** and **e**) Gene expression analysis of thermogenesis and beige cell markers in eWAT (**d**) and iWAT tissues (**e**) ($n = 6$ for each genotype). (**f** and **g**) Gene expression analysis of lipolytic enzymes and glucose transporter in eWAT (**f**) and iWAT (**g**) tissues, respectively. (**h**) Serum triglyceride level in the mice with genotypes as shown ($n = 5$ for WT; $n = 3$ for *Ptch1$^{c/c}$;HOC-Cre*). Data are presented as mean ± S.E.M. (*$P < 0.05$; **$P < 0.01$; ***$P < 0.001$)

the *Ptch1$^{c/c}$;HOC-Cre* mutant WAT were markedly reduced (Figures 4k and l). More importantly, the expression of Ucp1 was also significantly reduced (Figures 4m and n). Altogether, our data demonstrate that upregulated Hh signaling in osteoblasts secrete PTHrP into the circulation and PTHrP mediates its effect in WAT for thermogenesis and WAT browning.

To determine the signaling mechanism how PTHrP leads to WAT browning, we first examined PKA/cAMP signaling in the WAT of our mutant mice, a major downstream signaling pathway regulated by PTHrP. As expected, the expression of CREB was strongly induced in the *Ptch1$^{c/c}$;HOC-Cre* mutant WAT and they were activated as shown by the increased phosphorylated CREB level (Figure 5a). Interestingly, Akt/Foxo signaling that has been shown to be negatively regulating adipocyte thermogenesis[18] was inhibited as demonstrated by the reduced phosphorylation level of Akt. As a result, Foxo1 was activated that led to increased expression of Ucp1. To further test that PTHrP specifically elicited these changes, we treated the differentiated 3T3L1 cells with PTHrP together with H89, a specific PKA inhibitor (Figures 5b and c). Consistent with the results of PTHrP-neutralizing antibody treatment (Figure 4g), H89 treatment abolished most of the effects induced by PTHrP for thermogenesis marker expressions (Figure 5b). Furthermore, the effects on PKA/cAMP and Akt/Foxo signaling pathways were ameliorated (Figure 5c). Collectively, our data indicate that PTHrP regulates Ucp1 expression through PKA/cAMP and Akt/Foxo signaling that results in WAT browning and increased fatty acid oxidation.

Hypoglycemia in the *Ptch1$^{c/c}$;HOC-Cre* mutant is independent of insulin secretion and bone-derived osteocalcin. It has been previously established that bone regulates glucose metabolism by bone-derived hormone osteocalcin[11,12] and given that adipose tissues also serve as a crucial integrator of glucose homeostasis, we investigated whether glucose metabolism is affected in the *Ptch1$^{c/c}$;HOC-Cre* mutant mice. We found that the fasting serum glucose level was significantly reduced in the mutant mice

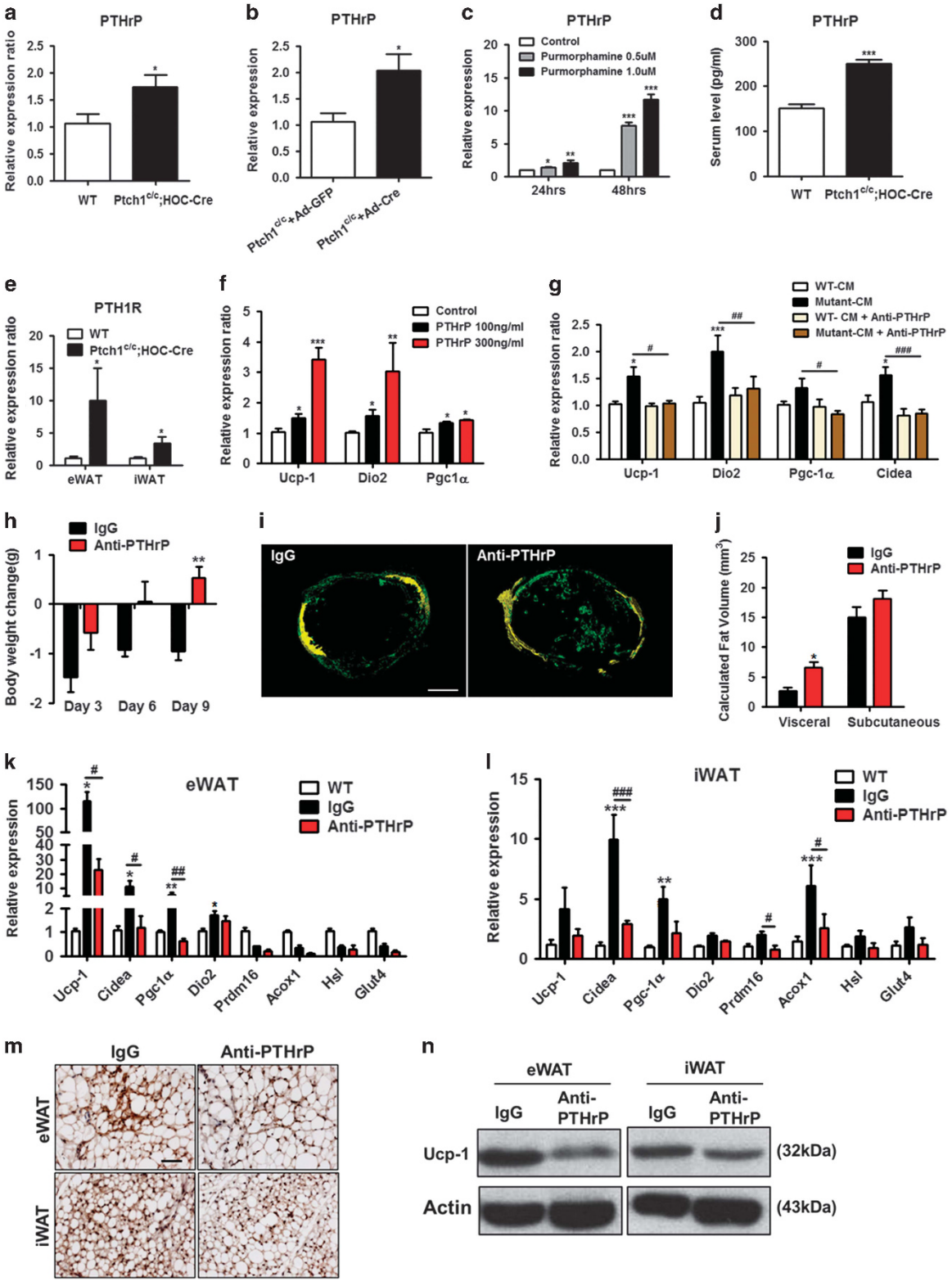

and glucose tolerance was improved in intraperitoneal glucose tolerance test (Figures 6a and b). Interestingly, the serum glucagon level was increased (Figure 6c) but no observable difference was detected in the fasting serum insulin level (Figure 6d). In addition, the serum level of bone-derived undercarboxylated osteocalcin was also reduced (Figure 6e). These data demonstrate that the hypoglycemic condition in our mutant mice is not due to increased

Figure 4 Bone-derived PTHrP contributes to WAT browning both *in vitro* and *in vivo*. (**a**) Gene expression of PTHrP in the bone tissues isolated from 2.5-month-old mouse femurs. ($n=5$ for each genotype). (**b**) PTHrP gene expression level in the *Ptch1$^{c/c}$* calvarial primary osteoblasts infected with *Cre-adenovirus*. *GFP- adenovirus* was used as control. (**c**) Gene expression of PTHrP in primary calvarial osteoblasts treated with 0.5 and 1.0 μM purmorphamine for 24 and 48 h respectively. (**d**) Serum PTHrP level of mice with genotypes as shown ($n=6$ for WT; $n=4$ for *Ptch1$^{c/c}$;HOC-Cre*). (**e**) Gene expression of PTH1R in the eWAT and iWAT tissues, respectively ($n=5$ for each genotype). (**f**) Gene expression analysis of differentiated 3T3L1 cells treated with 100 and 300 ng/ml recombinant PTHrP for 8 h, respectively. (**g**) Gene expression analysis of differentiated 3T3L1 cells treated with conditional medium and PTHrP-neutralizing antibody for 48 h as shown (* represents statistical analysis compared with WT-CM; # represents statistical analysis compared with Mutant-CM). (**h**) Body weight change of mutant mice during intraperitoneal injection of PTHrP-neutralizing antibody (4 mg/kg, every 3 days for a total of four times). IgG was used as a vehicle ($n=3$ for each group). (**i**) Cross images of μCT scan after the fourth round of PTHrP-neutralizing antibody injection of mutant mice. Green represents visceral fat depots and yellow represents subcutaneous fat depots (scale bar = 5 mm, $n=3$ for each group). (**j**) Quantification of fat depots as shown in (**i**). (**k** and **l**) Gene expression profiles of eWAT (**k**) and iWAT tissues (**l**) in mutant mice treated with IgG or anti-PTHrP antibody ($n=3$ for each group) (* represents statistical analysis compared with WT; # represents statistical analysis compared with mutant mice injected with IgG antibodies). (**m**) Representative images of Ucp1 expression in the eWAT and iWAT tissues of the mutant mice treated with IgG or anti-PTHrP antibody, respectively (scale bar = 50 μm, $n=3$ for each genotype). (**n**) Immunoblots of Ucp1 expression in the eWAT and iWAT tissues of the mutant mice ($n=3$ for each genotype). Data are presented as mean ± S.E.M. (* and $^{\#}$, $P<0.05$; ** and $^{\#\#}$, $P<0.01$; *** and $^{\#\#\#}$, $P<0.001$)

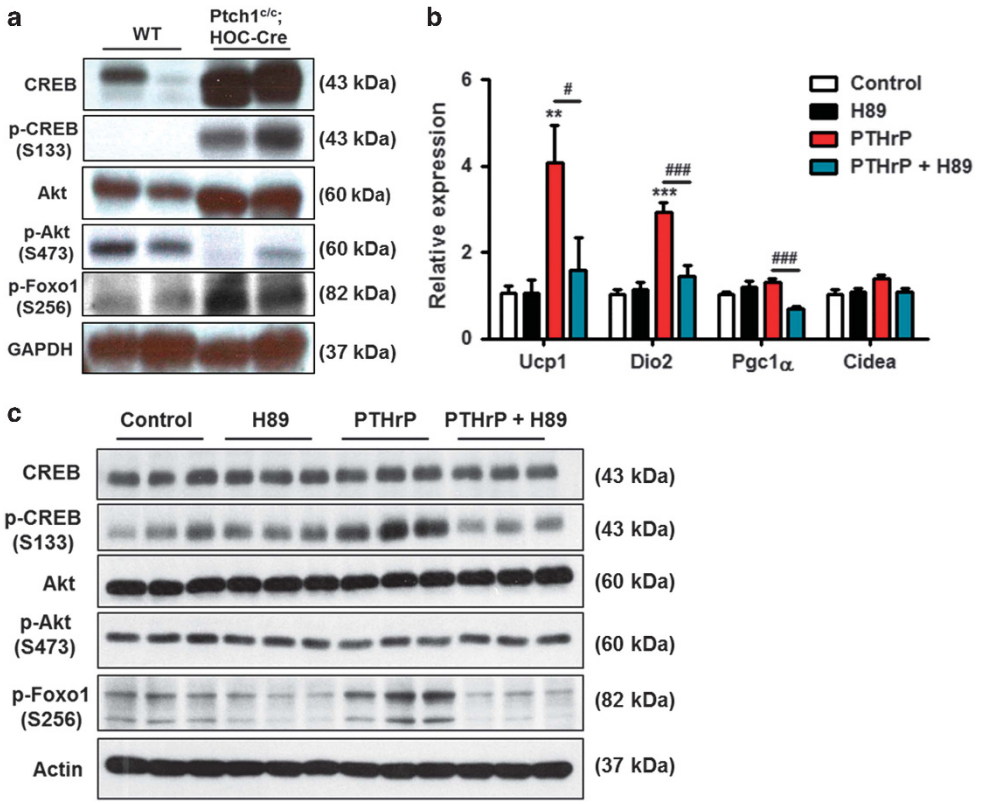

Figure 5 PTHrP activates both PKA and AKT signaling pathways in adipocytes both *in vivo* and *in vitro*. (**a**) Immunoblots of key components of PKA and AKT signaling pathways in the iWAT tissues as shown. (**b**) Gene expression analysis in differentiated 3T3L1 cells treated with PTHrP (100 ng/ml, 2 h) with or without H89 (30 μM, 1 h) pre-treatment (* represents statistical analysis compared with control; # represents statistical analysis compared with PTHrP treatment). (**c**) Immunoblots of key components of PKA and AKT signaling pathway in differentiated 3T3L1 cells treated with PTHrP (100 ng/ml, 30 min) with or without H89 (30 μM, 1 h) pre-treatment. Data are presented as mean ± S.E.M. ($^{\#}P<0.05$; $^{**}P<0.01$; *** and $^{\#\#\#}$, $P<0.001$)

production of insulin and it is independent of bone-derived osteocalcin.

It has been shown that pancreas specific overexpression of PTHrP increases islet cell sizes and cell proliferation.[19] Thus, we examined the histology of the pancreas of our mutant mice. Surprisingly, no enlargement of islet cell size was observed (Figures 6f and g). Glucagon expression was increased but insulin expression was comparable to wild type (Figure 6h). These data were consistent with the measured serum parameters (Figures 6c and d) and suggest that bone-secreted PTHrP into the circulation may not be high enough to induce ectopic insulin secretion. However, when PTHrP-neutralizing antibodies were injected into the mutant mice, the circulating blood glucose level was significantly improved as compared with the IgG group (Figure 6i), while PTHrP-neutralizing antibodies has no effect in wild-type mice (Supplementary Figure S2b). This result suggests that PTHrP triggers the secretion of other hormones or adipokines that may improve insulin sensitivity or suppress glucose production.

Next, we tested whether increased fat content intake is able to rescue the hypoglycemic condition in the mutant

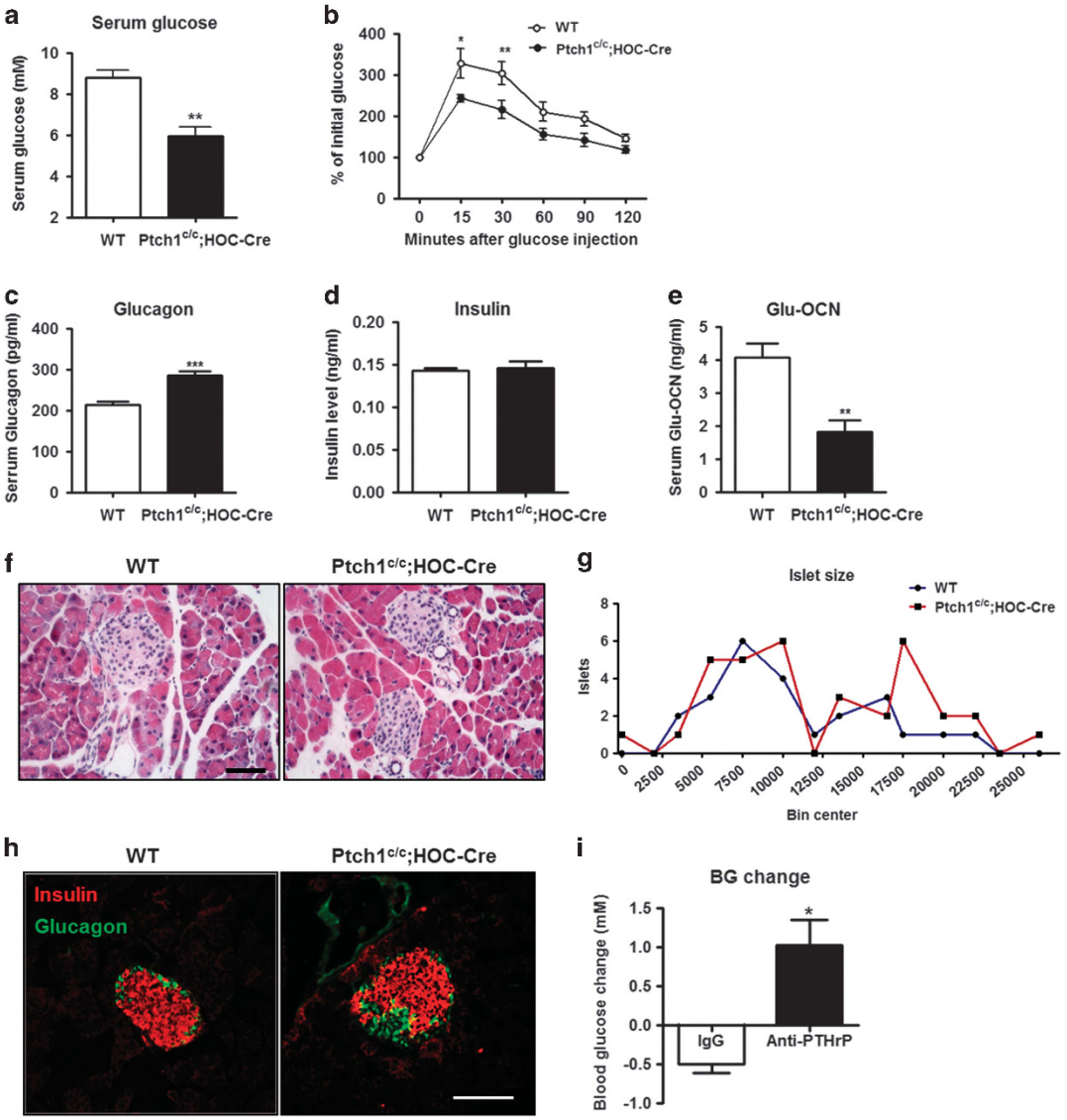

Figure 6 Hypoglycemic in the *Ptch1$^{c/c}$;HOC-Cre* mice is independent of bone-derived osteocalcin and insulin secretion. (**a**) Fasting serum glucose level in mice with genotypes as shown at 6-week-old ($n=4$ for each genotype). (**b**) IPGTT analysis in mice at 6 weeks old ($n=4$ for each genotype). (**c**) Serum glucagon level at 6 weeks old. (**d**) Serum insulin level in mice at 3 weeks old. (**e**) Serum Glu-osteocalcin level in mice at 6 weeks old ($n=5$ for each genotype). (**f**) Representative images of H&E staining of pancreas islets in mice with genotypes as shown (scale bar = 50 μm, $n=3$ for each genotype). (**g**) Islet size distribution of the entire pancreas in mice. H&E sections of pancreas were analyzed by Image J software (24 islets were counted for wild-type mice; 34 islets were counted for mutant mice). (**h**) Representative images of immunofluorescent staining of insulin and glucagon expression in the pancreatic islets of mice with genotypes as shown (scale bar = 100 μm, $n=3$ for each genotype). (**i**) Fasting blood glucose level after intraperitoneal injection of PTHrP-neutralizing antibody. IgG was used as a control for comparison ($n=3$ for each group). Data are presented as mean ± S.E.M. (*$P<0.05$; **$P<0.01$; ***$P<0.001$)

mice. We treated the mice with high-fat diet (HFD) for 1 month and analyzed their glucose homeostasis parameters (Supplementary Figures S3a and b). Our results showed that both the body weight gain and the circulating blood glucose level were significantly improved in the mutant group when treated with HFD. However, the expression levels of thermogenesis markers in WAT were not affected (Supplementary Figure S3c). Specifically, the Ucp1 level was not changed upon HFD treatment (Supplementary Figures S3c and d). These data indicate that hypoglycemia is secondary to the increased fatty acid oxidation and WAT browning.

Bone-derived PTHrP induces adiponectin secretion in WAT. Neutralization of circulating PTHrP improved hypoglycemic condition in the mutant mice but bone-derived PTHrP has no effects on insulin and osteocalcin secretion. It suggests that other hormones may interfere the action of PTHrP in WAT that is responsible for glucose homeostasis. In our *Ptch1$^{c/c}$;HOC-Cre* mutant mice, since bone homeostasis

was perturbed,[17] we examined the effects of major osteokines in adipose tissue metabolism (Supplementary Figure S4). We found that the expression of major osteokines tested were either no change or reduced in the bone tissues, suggesting that they are not ectopically secreted into the circulation (Supplementary Figure S4a). In addition, treating differentiated 3T3L1 adipocyte cell lines with these osteokines showed no significant change of expression profiles of thermogenesis markers (Supplementary Figures S4b–d). Rankl was induced in the mutant bone tissues,[17] but it also showed no effect in adipose tissues (Supplementary Figure 4e). Thus, we ruled out the possibility of osteokines in regulating WAT metabolism. Next, we asked whether adipokines were affected by PTHrP. We measured serum levels of major adipokines (Supplementary Figure S5 and Figure 7a). Among all the adipokines tested, only the adiponectin level was significantly increased (Figure 7a). Both the RNA and protein levels of adiponectin were upregulated in the mutant WAT (Figures 7b–d). Adiponectin is an insulin-sensitizing hormone, which is involved in the regulation of glucose homeostasis.[20–22] Thus, we tested whether PTHrP has any effect in regulating adiponectin expression. When 3T3L1 adipocytes were treated with conditioned medium isolated from the mutant bone chips, *Adiponectin* expression was significantly induced (Figure 7e). Upon PTHrP-neutralizing antibodies injection *in vivo*, the expression level of *Adiponectin* in the *Ptch1$^{c/c}$;HOC-Cre* WAT tissues was greatly reduced (Figure 7f), suggesting that PTHrP stimulates adiponectin secretion. Thus, we treated differentiated 3T3L1 cells with recombinant PTHrP and found that adiponectin was increased (Figure 7g). Furthermore, we also collected culture medium from the 3T3L1 cells after PTHrP treatment and examined the secretion of adiponectin (Figure 7h). We found that the increased expression of adiponectin also resulted in increased secretion of adiponectin from the 3T3L1 cells. To demonstrate that the secretion of adiponectin is a specific effect of PTHrP, we co-treated PTHrP with H89, a specific inhibitor of PKA signaling. We found that the expression of both adiponectin and its receptors were greatly induced by PTHrP treatment alone, but reduced significantly when treated together with H89 treatment (Figure 7i). Adiponectin secretion was similarly reduced in the condition medium (Figure 7j). Altogether, our data indicate that PTHrP stimulates adiponectin secretion in WAT.

Adiponectin induces skeletal muscle atrophy and hepatic fatty acid oxidation. Apart from WAT browning, the body lean mass was also significantly reduced in our *Ptch1$^{c/c}$; HOC-Cre* mutant mice (Figure 2a). Since skeletal muscles also contribute to energy metabolism, we therefore also examined whether skeletal muscles were affected in the mutant mice. Interestingly, histologic examination revealed that skeletal muscle size was obviously smaller in the mutant samples (Figures 8a and b). More importantly, skeletal muscle atrophy-associated marker genes (*Mstn, Fbxo32, Trim63*) were all strongly upregulated (Figure 8c). In addition, the expression of the main receptor of adiponectin in the skeletal muscles *AdipoR1* was also significantly increased (Figure 8d), suggesting that adiponectin stimulates fatty acid oxidation in the skeletal muscles. Consistently, PPARα target genes that involved in fatty acid oxidation (*Aco, Cpt1, Fabp3*) and glucose transporters responsible for glucose uptake (*Glut1, Glut4*) were all significantly upregulated (Figure 8e). Since the action of adiponectin is primarily mediated by the activation of 5′-AMP-activated protein kinase (AMPK),[23,24] we examined the activity of the AMPK/ACC pathway. As expected, both AMPK and acetyl-coA carboxylase (ACC) were strongly phosphorylated in the mutant skeletal muscles, indicating that fatty acid oxidation was increased in the mutant skeletal muscles (Figure 8f). In addition, AMPK was also activated in the liver (Supplementary Figure S6a) and the expression of *Glut1* was significantly increased (Supplementary Figure S6b). Furthermore, the expression of enzymes responsible for hepatic glucose production *G6Pase* was markedly reduced (Supplementary Figure S6c). These data indicate that Adiponectin increases hepatic fatty acid oxidation and inhibits hepatic glucose production. Altogether, PTHrP couples Adiponectin actions to induce systemic fatty acid oxidation and glucose uptake that leads to hypoglycemia. In summary, our results strongly indicate that upregulated Hh signaling from bone increases systemic whole-body energy metabolism through a bone–adipose endocrine relay mediated by PTHrP and Adiponectin.

Discussion

Here, we uncovered a previously unappreciated role of Hh signaling in bone for whole-body metabolism. In addition to the non-cell autonomous role of Hh signaling and its paracrine actions on bone resorption, we found that Hh signaling also induces bone-derived PTHrP to influence systemic energy expenditure by targeting adipose tissues (Supplementary Figure S7). Our study established a novel bone–adipose endocrine axis in regulating whole-body energy metabolism.

Bone acquisition and bone remodeling are energy expensive processes. As upregulated Hh signaling in mature osteoblasts causes continuous acceleration of bone remodeling,[17] a high demand of energy is required during this process. Our results show that overall fat content is significantly reduced, normal level of glucose cannot be maintained and skeletal muscle atrophy is observed. All these effects are initiated by the endocrine action of bone-derived PTHrP that elicits WAT browning for thermogenesis and subsequent release of adiponectin that enhances systemic *β*-oxidation.

The pleiotropic effects of PTH/PTHrP signaling have been widely described in bone formation,[25–27] bone resorption[17,28] and bone metastasis.[29,30] More recently PTHrP is also implicated in cancer-induced cachexia.[31] By using a Lewis lung carcinoma model, Kir *et al.* showed that tumor-derived PTHrP induces cachexia, which phenocopies to the metabolic phenotypes observed in our *Ptch1$^{c/c}$;HOC-Cre* mutant mice. The tumor-bearing mice displayed evident weight loss; enhanced oxygen consumption and energy expenditure; WAT browning and muscle wasting. All these metabolic changes are attributed to the secretion of PTHrP into circulation by the tumor mass. Our study demonstrates that in whole-body physiology, bone-derived, in contrast to tumor-

derived, PTHrP is also able to induce WAT browning and enhance energy expenditure. We further demonstrate that bone-derived PTHrP stimulates Adiponectin in WAT to elicit systemic metabolic changes. This finding unravels another regulatory axis between the bone and adipose tissue in whole-body physiology.

PTHrP has been tested in clinical trials as an anabolic agent for bone formation in treating patients with osteoporosis.[32,33]

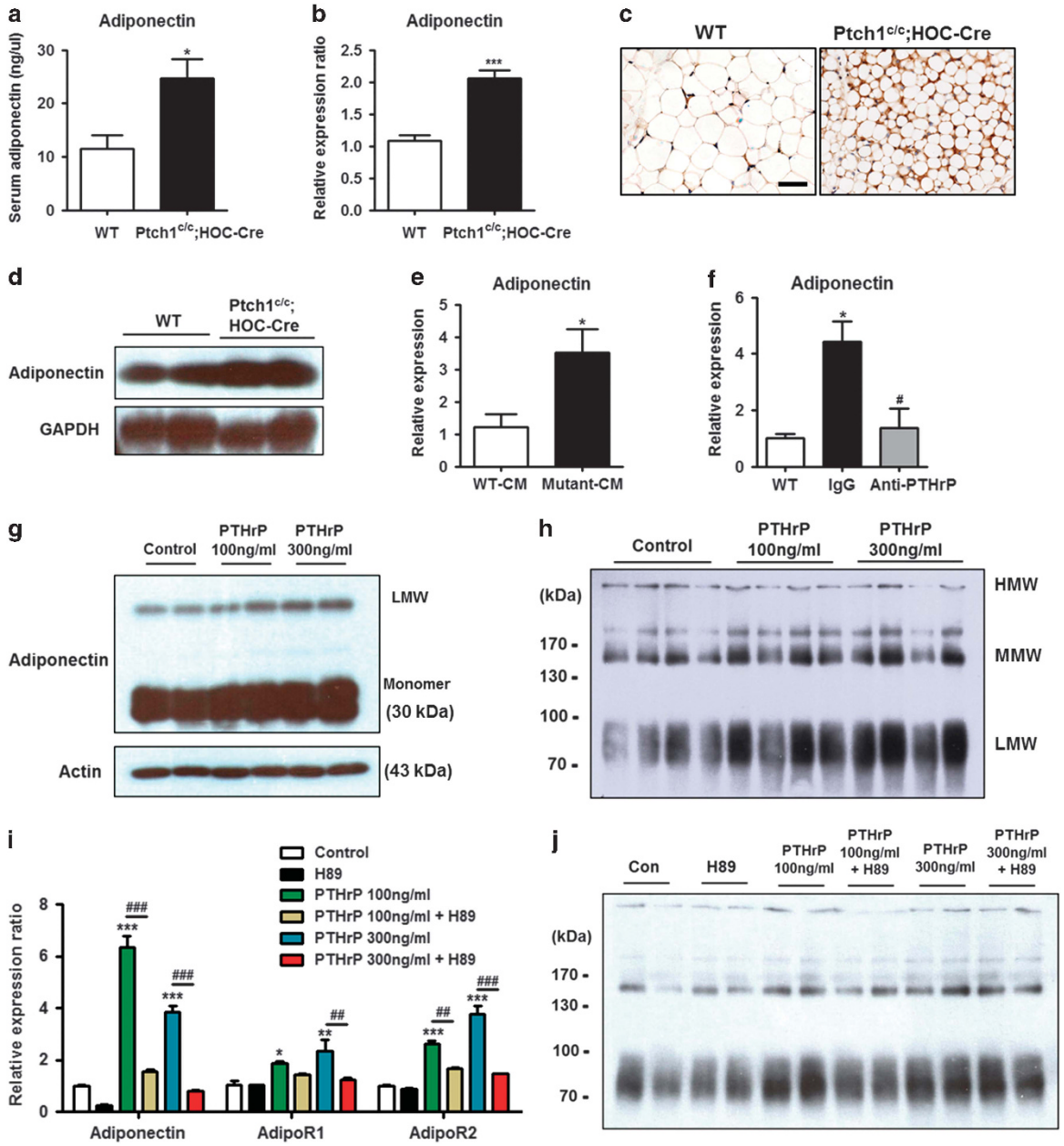

Figure 7 PTHrP stimulates adiponectin expression and secretion in WAT. (**a**) Serum adiponectin level in mice with genotypes as shown ($n=4$ for WT; $n=3$ for *Ptch1$^{c/c}$;HOC-Cre*). (**b**) Gene expression of *Adiponectin* in the iWAT tissues. (**c**) Representative images of immunostaining of Adiponectin expression in the iWAT tissues (scale bar = 50 μm, $n=3$ for each genotype). (**d**) Immunoblots of Adiponectin protein expression in the iWAT tissues ($n=3$ for each genotype). (**e**) Gene expression of *Adiponectin* in differentiated 3T3L1 cells after conditioned medium treatment isolated from the *Ptch1$^{c/c}$;HOC-Cre* mutant bone chips. (**f**) Gene expression of *Adiponectin* in the iWAT tissues of mutant mice after IgG or Anti-PTHrP antibody treatment (* represents statistical analysis compared with WT; # represents statistical analysis compared with mutant mice injected with anti-PTHrP antibodies). (**g**) Immunoblots of Adiponectin protein expression (monomer and low molecular weight) of differentiated 3T3L1 cells treated with 100 and 300 ng/ml recombinant PTHrP for 72 h. (**h**) Immunoblots of Adiponectin expression (low-, middle-, high-molecular weight) in the culture medium collected from differentiated 3T3L1 cells treated with 100 and 300 ng/ml recombinant PTHrP for 72 h. (**i**) Gene expression analysis of differentiated 3T3L1 cells treated with 100 and 300 ng/ml recombinant PTHrP for 72 h with or without pre-treatment of H89 (10 μM, 1 h) (* represents statistical analysis compared with control; # represents statistical analysis compared with 100 or 300 ng/ml PTHrP treatment, respectively). (**j**) Immunoblots of Adiponectin expression in the culture medium collected from differentiated 3T3L1 cells treated with 100 and 300 ng/ml recombinant PTHrP for 72 h with or without pre-treatment of H89 (10 μM, 1 h). Data are presented as mean ± S.E.M. (* and $^{\#}$, $P<0.05$; ** and $^{\#\#}$, $P<0.01$; *** and $^{\#\#\#}$, $P<0.001$)

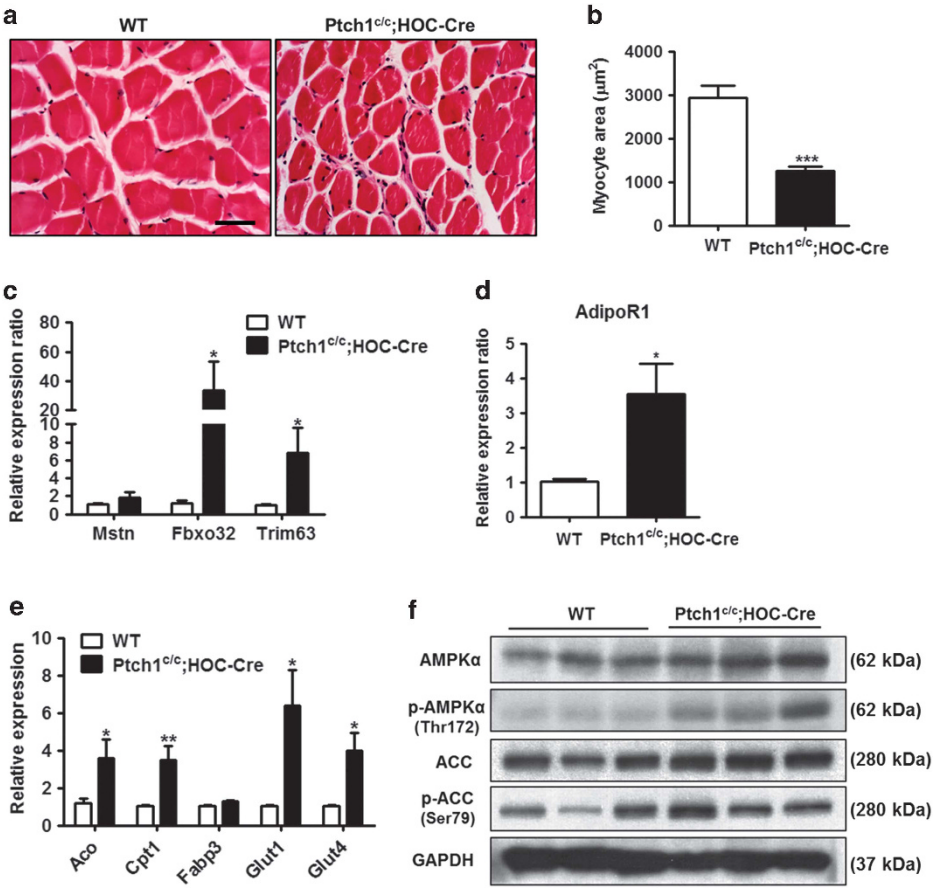

Figure 8 Skeletal muscle defects in the *Ptch1$^{c/c}$; HOC-Cre* mutant mice. (**a**) Representative images of H&E staining of quadriceps femoris muscles in mice with genotypes as shown (scale bar = 50 μm, $n = 3$ for each genotype). (**b**) Quantification of muscle fiber size as shown in (**a**). (**c**) Muscle atrophy-associated gene expressions analysis ($n = 3$ for each genotype). (**d**) Gene expression of *AdipoR1* in the iWAT tissues ($n = 3$ for each genotype). (**e**) Gene expression analysis of β-oxidation-associated genes and glucose transporters in the skeletal muscles in mice ($n = 3$ for each genotype). (**f**) Immunoblots of protein expression in the AMPK pathway in skeletal muscle tissues. Data are presented as mean ± S.E.M. (*$P < 0.05$; **$P < 0.01$; ***$P < 0.05$)

However, it remains to be elucidated the differential outcomes and molecular mechanisms between intermittent and continuous administration of PTHrP. Of note, so far all the studies related to PTHrP therapies only focus on the change of bone mass, but no detail information is reported concerning glucose and energy metabolism in these osteoporotic patients. It is reported that circulating osteocalcin is increased after PTHrP administration,[32] but it remains to be determined whether insulin sensitivity and energy expenditure are also affected in these patients. Our findings open up a new avenue that integrates bone metabolism and energy expenditure. In the future, a broader perspective should be evaluated when considering the use of PTHrP for treating osteoporotic patients. In particular, it may be beneficial to osteoporotic patients who also suffer with energy metabolic defects such as diabetes.

Our findings reveal that adiponectin secretion is regulated by PTHrP in WAT. Previous studies show that adiponectin suppresses triglyceride accumulation, increases fatty acid oxidation and activates AMP kinase in skeletal muscle and thus, improving insulin signaling.[23,24] Adiponectin also suppresses glucose production and activates AMPK in the liver.[20–22] All these metabolic phenotypes were observed in our *Ptch1$^{c/c}$;HOC-Cre* mutant mice. However, increased adiponectin secretion did not result in increased insulin secretion in our mutant mice, albeit insulin sensitivity is enhanced. This may be reconciled by the fact that the circulating glucose level is very low in our mutant mice, which inhibits the production and secretion of insulin from the pancreas. It has been suggested that adiponectin causes insulin secretion from β-cells only in the presence of a relatively high level of glucose *in vitro*.[34,35] In our mutant mice, however, circulating glucose levels were consistently low and thus, insulin secretion is inhibited.

In summary, our work establishes a new bone–adipose axis in regulating whole-body metabolism, which is mediated by PTHrP and adiponectin. Our findings provide new insights for the development of therapeutic treatment for patients with both bone and metabolic diseases.

Materials and Methods

Reagent. ELISA Kit for Parathyroid Hormone Related Protein (PTHrP) (SEA819Mu) and recombinant PTHrP (RPA819Mu01) were purchased from Wuhan USCN Business Co., Ltd (Wuhan, China). ELISA Kit for insulin (Cat. 32282) and

adiponectin (Cat. 32010) were purchased from Antibody and Immunoassay Services, HKU (Pokfulam). The anti-PTHrP (1-34) IgG (T-4512) was purchased from Peninsula Laboratories International, Inc. (San Carlos, CA, USA) Normal rabbit IgG (Santa Cruz Biotechnology (Dallas, TX, USA); sc-2027) was used as a control for the anti-PTHrP antibody. All other antibodies were purchased from Cell Signaling Technology (Davers, MA, USA), including rabbit antibodies specific for CREB (#9197S), phospho-CREB (#9198), Akt (#4691S), phosphor-Akt (#4060P) and AMPK and ACC antibody sampler kit (#9957S). Anti-UCP1 (GTX112784) was purchased from GeneTex (Irvine, CA, USA) and anti-GAPDH (sc-25778) from Santa Cruz (Dallas, TX, USA).

Mice. The *Ptch1$^{c/c}$* mice carrying the floxed alleles of Ptch1[36] were crossed with the human Osteocalcin-Cre (HOC-Cre) mice[37] to generate the *Ptch1$^{c/c}$;HOC-Cre* mice as previously described.[17] Male mice with the age of 8- to 12 week-old were used in most of the experiments. Their littermates with the genotypes of *Ptch1$^{c/c}$* or *Ptch1$^{c/+}$* were used as controls. For HFD treatment, mice were fed with standard chow or an HFD containing 60% fat (Research Diets, New Brunswick, NJ, USA) *ad libitum* for 4 weeks. Mice were housed on a 12 : 12 h light : dark cycle. All experiments were approved by the Animal Experimentation Ethics Committee of the Chinese University of Hong Kong.

Metabolic cage. Whole-body oxygen consumption and heat production were measured using the comprehensive laboratory animal monitoring system (CLAMS; Columbus Instruments, Columbus, OH, USA). Briefly, mice were housed individually in CLAMS cages and acclimated for 48 h, and data of oxygen consumption (VO_2), carbon dioxide production (VCO_2), respiratory exchange ratio and locomotor activity levels were recorded every 10 min for a 48-h period with temperature at 22 °C.

Whole-body composition analysis and micro-CT analysis. Total fat and lean mass of the mice were measured by the minispec LF90 TD-NMR analyser (Bruker Corporation, Billerica, MA, USA). Mice were weighed just before placing into the sampling compartment for analysis. Adiposity is calculated as the percentage of fat/(fat+lean mass). For micro-CT analysis, mice were perfused and fixed in 4% PFA by cardiac perfusion. For quantification of adipose tissue, the whole-body trunk of the mouse was scanned by micro-CT (μCT40; Scanco Medical, Bruttisellen, Switzerland) using the following settings: voxel size of 37 μm, 45 kVp, 177 μA, medium resolution and 200 ms integration time. The abdominal region from L1 to L5 vertebrae was chosen for three-dimensional (3D) reconstruction and quantification of visceral and subcutaneous fat tissues using the software of Analyze 12.0 (AnalyzeDirect, Inc., Chicago, IL, USA). The detailed quantification method was described previously.[38,39] For analysis of bone, the whole tibia was isolated and scanned by micro-CT with a resolution of 7 μm, isometric voxel 70 kVp and 114 μA. The 3D reconstruction was performed for the regions of interest and subjected to bone microarchitecture and mineral density analyses using built-in software from Scan Medical Ltd (Frimley Camberley, Surrey, UK) and published protocol.[40]

Quantification of adipocyte area and frequency and myocyte area. Three representative photos of each section from three individual mice were chosen for quantification of adipocyte area and frequency and myocyte area using MetaMorph image analysis software (Molecular Devices, LLC, Sunnyvale, CA, USA). The detailed protocol was described previously.[41]

PTHrP-neutralizing antibody injection. Mice received 4 mg/kg IgG (Santa Cruz Biotechnology; sc-2027) or anti-PTHrP (1-34) neutralizing antibody (Peninsula Laboratories International, Inc; T-4512) through intraperitoneal injection every 3 days for four times. Body weight and the fasting (6 h) blood glucose level were measured just before the injection and the next day after the last injection. Mice were then dissected for blood serum and adipose tissue was collected on day 11.

Primary cell isolation and treatment. Calvaria were harvested from P1 to P3 newborn pups of *Ptch1$^{c/c}$* mice. Soft tissue was removed and the calvaria were washed in PBS and subjected to five sequential digestions by 0.5% collagenase (Roche, Hong Kong, China) in a-MEM medium at 37 °C for 25 min each. The cells from the last four digestions were collected and expanded for subsequent cultures. Primary osteoblasts of *Ptch1$^{c/c}$* mice were infected with *Cre-adenovirus* or *GFP-adenovirus*. Culture medium was changed after 16 h infection. Then the infected cells were cultured for another 2 days before collection for further analysis. For purmorphamine treatment, primary cultured osteoblasts were serum starved overnight, then treated with purmorphamine at a final concentration of 0.5 or 1.0 μM. Cells were collected after 24 or 48 h treatment. 3T3L1 cells (ATCC, Manassas, VA, USA) were differentiated by an induction medium containing 0.02 μM insulin, 1 nM T3, 125 μM indomethacin, 0.5 μM isobutylmethylxanthine (IBMX) and 5 μM dexamethasone. After 2 days induction, cells were maintained in adipocyte culture medium containing 0.02 μM insulin and 1 nM T3 for 8 days. Differentiated 3T3L1 cells were used for further experiments.

Conditioned medium preparation. Cortical bones from the femurs were collected. Bones were cut into small pieces and equal weights of bone chips from individual mice were cultured in a 24-well plate with serum-free a-MEM medium, respectively. Conditioned medium was collected every 24 h for 3 days and pooled together. During treatment, 75% of conditioned medium was mixed with 25% fresh adipocyte culture medium.

Quantitative RT-PCR. RNA was extracted from cultured cells or frozen tissue samples using TRIzol (Invitrogen HK Ltd, China) and reverse-transcribed to cDNA using the M-MLV Reverse Transcriptase (Thermo Fisher Scientific, HK, China). Resulting cDNA was analyzed by qPCR using Power SYBR Green PCR Master Mix (Applied Biosystems, Carlsbad, CA, USA). Reactions were performed in 384-well format using an ABI PRISM 7900HT instrument (Applied Biosystems). Relative mRNA levels were calculated using the comparative CT method and normalized to actin and β-tubulin mRNA. The sequence information of the mouse primer sets is listed in Supplementary Table S1.

Immunohistochemistry. Adipose tissue samples were fixed in 4% PFA, dehydrated and embedded in paraffin. Sections (10 μm) were boiled in TE buffer for 20 min for antigen retrieval and then incubated with blocking serum for 1 h at room temperature followed by incubation of primary antibodies: Ucp1 (1:100, anti-rabbit; GeneTax), Adiponectin (1:100, anti-rabbit; AIS, HKU, Pokfulam) at 4 °C overnight. Biotinated secondary antibodies were added to the sections and incubated for 30 min. Avidin–biotin–peroxidase complex was formed by using the Vectastain Elite ABC Kit (Vector Laboratories, Inc., Burlingame, CA, USA) for 30 min. Signals were developed using 3,3-diaminobenzidine tetra-hydrochloride (2-solution DAB kit; Life Technologies Corporation, Carlsbad, CA, USA).

Western blotting. The adipose tissue and skeletal muscle samples were homogenized in RIPA buffer containing 150 mM sodium chloride, 1.0% NP-40, 0.5% sodium deoxycholate, 0.1% SDS (sodium dodecyl sulfate) and 50 mM Tris, pH 8.0, supplemented with 1 mM phenylmethylsulphonyl fluoride and protease inhibitor cocktails (Roche). The supernatant was collected and protein concentration was measured by BCA assay. Protein samples (40 μg) were separated by SDS-PAGE and transferred to polyvinylidene difluoride membrane. After blocking with 5% non-fat dry milk or BSA in 1× TBST buffer, membranes were hybridized with appropriate primary antibodies: CREB (1:1000, anti-rabbit; Cell Signaling), p-CREB (S133, 1:1000; anti-rabbit), Akt (1:2000, anti-rabbit; Cell Signaling), p-Akt (S473) (1:1000, anti-rabbit; Cell Signaling), p-Foxo1 (S256) (1:1000, anti-rabbit; Cell Signaling), AMPKa (1:1000, anti-rabbit; Cell Signaling), p-AMPKa (Thr172) (1:1000, anti-rabbit; Cell Signaling), ACC (1:1000, anti-rabbit; Cell Signaling), p-ACC (Ser79) (1:1000, anti-rabbit; Cell Signaling), GAPDH (1:1000, anti-rabbit; Santa Cruz), Ucp1 (1:1000, anti-rabbit; GeneTax) overnight. Then, the membranes were incubated with HRP-conjugated secondary anti-rabbit IgG (1 : 5000) for 1 h. Protein signals were visualized with the ECL (PerkinElmer, Waltham, MA, USA) system.

Statistical analysis. The values are expressed as mean ± S.E.M. Statistical analysis was performed using two-tailed, unpaired *t*-test for single variables and two-way ANOVA followed by Bonferonni post-tests for multiple variables. *P*-values ≤ 0.05 were considered statistically significant. Graphpad Prism software was used for *t*-test and *ANOVA* analysis. No statistical method was used to predetermine sample size. Samples were not randomized. The inclusion criteria were the appropriate genotype of the mice. At least three independent experiments were performed for all biochemical experiments and representative images were shown.

Conflict of Interest

The authors declare no conflict of interest.

Acknowledgements. We thank members of the Mak lab for stimulating discussions. We thank Drs Yu Huang, School of Biomedical Sciences, The Chinese University of Hong Kong for sharing of reagents, Aimin Xu, Department of Pharmacology & Pharmacy, The University of Hong Kong for sharing the CLAM system. This work is supported by the Seed Fund of the School of Biomedical Sciences, The Chinese University of Hong Kong (4620504), SBS group research grant, The Chinese University of Hong Kong (BL12986), Direct grant for research from Research Grant Council, Hong Kong (BL12615), Guangdong Science and Technology Bureau International Science and Technology Collaboration Program (20130501c).

Author contributions

XZ designed and performed most of the experiments; QC and PL designed and performed experiments related to glucose homeostasis; YW performed NMR analysis; KKM analyzed, interpreted data and supervised the project; and XZ and KKM wrote the manuscript.

1. Kelly AS, Barlow SE, Rao G, Inge TH, Hayman LL, Steinberger J *et al.* Severe obesity in children and adolescents: identification, associated health risks, and treatment approaches: a scientific statement from the American Heart Association. *Circulation* 2013; **128**: 1689–1712.
2. Demmer RT, Zuk AM, Rosenbaum M, Desvarieux M. Prevalence of diagnosed and undiagnosed type 2 diabetes mellitus among US adolescents: results from the continuous NHANES, 1999-2010. *Am J Epidemiol* 2013; **178**: 1106–1113.
3. Kawai M, de Paulaes FJ, Rosen CJ. New insights into osteoporosis: the bone-fat connection. *J Intern Med* 2012; **272**: 317–329.
4. Zhao LJ, Jiang H, Papasian CJ, Maulik D, Drees B, Hamilton J *et al.* Correlation of obesity and osteoporosis: effect of fat mass on the determination of osteoporosis. *J Bone Miner Res* 2008; **23**: 17–29.
5. Janicka A, Wren TA, Sanchez MM, Dorey F, Kim PS, Mittelman SD *et al.* Fat mass is not beneficial to bone in adolescents and young adults. *J Clin Endocrinol Metab* 2007; **92**: 143–147.
6. Forsen L, Meyer HE, Midthjell K, Edna TH. Diabetes mellitus and the incidence of hip fracture: results from the Nord-Trondelag Health Survey. *Diabetologia* 1999; **42**: 920–925.
7. Schwartz AV, Sellmeyer DE, Ensrud KE, Cauley JA, Tabor HK, Schreiner PJ *et al.* Older women with diabetes have an increased risk of fracture: a prospective study. *J Clin Endocrinol Metab* 2001; **86**: 32–38.
8. Lee NK, Sowa H, Hinoi E, Ferron M, Ahn JD, Confavreux C *et al.* Endocrine regulation of energy metabolism by the skeleton. *Cell* 2007; **130**: 456–469.
9. Ferron M, Hinoi E, Karsenty G, Ducy P. Osteocalcin differentially regulates beta cell and adipocyte gene expression and affects the development of metabolic diseases in wild-type mice. *Proc Natl Acad Sci USA* 2008; **105**: 5266–5270.
10. Oury F, Sumara G, Sumara O, Ferron M, Chang H, Smith CE *et al.* Endocrine regulation of male fertility by the skeleton. *Cell* 2011; **144**: 796–809.
11. Ferron M, Wei J, Yoshizawa T, Del Fattore A, DePinho RA, Teti A *et al.* Insulin signaling in osteoblasts integrates bone remodeling and energy metabolism. *Cell* 2010; **142**: 296–308.
12. Fulzele K, Riddle RC, DiGirolamo DJ, Cao X, Wan C, Chen D *et al.* Insulin receptor signaling in osteoblasts regulates postnatal bone acquisition and body composition. *Cell* 2010; **142**: 309–319.
13. Yoshikawa Y, Kode A, Xu L, Mosialou I, Silva BC, Ferron M *et al.* Genetic evidence points to an osteocalcin-independent influence of osteoblasts on energy metabolism. *J Bone Miner Res* 2011; **26**: 2012–2025.
14. St-Jacques B, Hammerschmidt M, McMahon AP. Indian hedgehog signaling regulates proliferation and differentiation of chondrocytes and is essential for bone formation. *Genes Dev* 1999; **13**: 2072–2086.
15. Vortkamp A, Lee K, Lanske B, Segre GV, Kronenberg HM, Tabin CJ. Regulation of rate of cartilage differentiation by Indian hedgehog and PTH-related protein. *Science* 1996; **273**: 613–622.
16. Ohba S, Kawaguchi H, Kugimiya F, Ogasawara T, Kawamura N, Saito T *et al.* Patched1 haploinsufficiency increases adult bone mass and modulates Gli3 repressor activity. *Dev Cell* 2008; **14**: 689–699.
17. Mak KK, Bi Y, Wan C, Chuang PT, Clemens T, Young M *et al.* Hedgehog signaling in mature osteoblasts regulates bone formation and resorption by controlling PTHrP and RANKL expression. *Dev Cell* 2008; **14**: 674–688.
18. Ortega-Molina A, Efeyan A, Lopez-Guadamillas E, Munoz-Martin M, Gomez-Lopez G, Canamero M *et al.* Pten positively regulates brown adipose function, energy expenditure, and longevity. *Cell Metab* 2012; **15**: 382–394.
19. Vasavada RC, Cavaliere C, D'Ercole AJ, Dann P, Burtis WJ, Madlener AL *et al.* Overexpression of parathyroid hormone-related protein in the pancreatic islets of transgenic mice causes islet hyperplasia, hyperinsulinemia, and hypoglycemia. *J Biol Chem* 1996; **271**: 1200–1208.
20. Combs TP, Berg AH, Obici S, Scherer PE, Rossetti L. Endogenous glucose production is inhibited by the adipose-derived protein Acrp30. *J Clin Invest* 2001; **108**: 1875–1881.
21. Berg AH, Combs TP, Du X, Brownlee M, Scherer PE. The adipocyte-secreted protein Acrp30 enhances hepatic insulin action. *Nat Med* 2001; **7**: 947–953.
22. Yamauchi T, Kamon J, Ito Y, Tsuchida A, Yokomizo T, Kita S *et al.* Cloning of adiponectin receptors that mediate antidiabetic metabolic effects. *Nature* 2003; **423**: 762–769.
23. Yamauchi T, Kamon J, Minokoshi Y, Ito Y, Waki H, Uchida S *et al.* Adiponectin stimulates glucose utilization and fatty-acid oxidation by activating AMP-activated protein kinase. *Nat Med* 2002; **8**: 1288–1295.
24. Tomas E, Tsao TS, Saha AK, Murrey HE, Zhang Cc C, Itani SI *et al.* Enhanced muscle fat oxidation and glucose transport by ACRP30 globular domain: acetyl-CoA carboxylase inhibition and AMP-activated protein kinase activation. *Proc Natl Acad Sci USA* 2002; **99**: 16309–16313.
25. Lanske B, Karaplis AC, Lee K, Luz A, Vortkamp A, Pirro A *et al.* PTH/PTHrP receptor in early development and Indian hedgehog-regulated bone growth. *Science* 1996; **273**: 663–666.
26. Lanske B, Amling M, Neff L, Guiducci J, Baron R, Kronenberg HM. Ablation of the PTHrP gene or the PTH/PTHrP receptor gene leads to distinct abnormalities in bone development. *J Clin Invest* 1999; **104**: 399–407.
27. Miao D, He B, Jiang Y, Kobayashi T, Soroceanu MA, Zhao J *et al.* Osteoblast-derived PTHrP is a potent endogenous bone anabolic agent that modifies the therapeutic efficacy of administered PTH 1-34. *J Clin Invest* 2005; **115**: 2402–2411.
28. Ma YL, Cain RL, Halladay DL, Yang X, Zeng Q, Miles RR *et al.* Catabolic effects of continuous human PTH (1–38) *in vivo* is associated with sustained stimulation of RANKL and inhibition of osteoprotegerin and gene-associated bone formation. *Endocrinology* 2001; **142**: 4047–4054.
29. Guise TA, Yin JJ, Taylor SD, Kumagai Y, Dallas M, Boyce BF *et al.* Evidence for a causal role of parathyroid hormone-related protein in the pathogenesis of human breast cancer-mediated osteolysis. *J Clin Invest* 1996; **98**: 1544–1549.
30. Sterling JA, Oyajobi BO, Grubbs B, Padalecki SS, Munoz SA, Gupta A *et al.* The hedgehog signaling molecule Gli2 induces parathyroid hormone-related peptide expression and osteolysis in metastatic human breast cancer cells. *Cancer Res* 2006; **66**: 7548–7553.
31. Kir S, White JP, Kleiner S, Kazak L, Cohen P, Baracos VE *et al.* Tumour-derived PTH-related protein triggers adipose tissue browning and cancer cachexia. *Nature* 2014; **513**: 100–104.
32. Plotkin H, Gundberg C, Mitnick M, Stewart AF. Dissociation of bone formation from resorption during 2-week treatment with human parathyroid hormone-related peptide-(1-36) in humans: potential as an anabolic therapy for osteoporosis. *J Clin Endocrinol Metab* 1998; **83**: 2786–2791.
33. Horwitz MJ, Tedesco MB, Garcia-Ocana A, Sereika SM, Prebehala L, Bisello A *et al.* Parathyroid hormone-related protein for the treatment of postmenopausal osteoporosis: defining the maximal tolerable dose. *J Clin Endocrinol Metab* 2010; **95**: 1279–1287.
34. Wijesekara N, Krishnamurthy M, Bhattacharjee A, Suhail A, Sweeney G, Wheeler MB. Adiponectin-induced ERK and Akt phosphorylation protects against pancreatic beta cell apoptosis and increases insulin gene expression and secretion. *J Biol Chem* 2010; **285**: 33623–33631.
35. Okamoto M, Ohara-Imaizumi M, Kubota N, Hashimoto S, Eto K, Kanno T *et al.* Adiponectin induces insulin secretion *in vitro* and *in vivo* at a low glucose concentration. *Diabetologia* 2008; **51**: 827–835.
36. Mak KK, Chen MH, Day TF, Chuang PT, Yang Y. Wnt/beta-catenin signaling interacts differentially with Ihh signaling in controlling endochondral bone and synovial joint formation. *Development* 2006; **133**: 3695–3707.
37. Zhang M, Xuan S, Bouxsein ML, von Stechow D, Akeno N, Faugere MC *et al.* Osteoblast-specific knockout of the insulin-like growth factor (IGF) receptor gene reveals an essential role of IGF signaling in bone matrix mineralization. *J Biol Chem* 2002; **277**: 44005–44012.
38. Luu YK, Lublinsky S, Ozcivici E, Capilla E, Pessin JE, Rubin CT *et al. In vivo* quantification of subcutaneous and visceral adiposity by micro-computed tomography in a small animal model. *Med Eng Phys* 2009; **31**: 34–41.
39. Judex S, Luu YK, Ozcivici E, Adler B, Lublinsky S, Rubin CT. Quantification of adiposity in small rodents using micro-CT. *Methods* 2010; **50**: 14–19.
40. Zhang G, Guo B, Wu H, Tang T, Zhang BT, Zheng L *et al.* A delivery system targeting bone formation surfaces to facilitate RNAi-based anabolic therapy. *Nat Med* 2012; **18**: 307–314.
41. Parlee SD, Lentz SI, Mori H, MacDougald OA. Quantifying size and number of adipocytes in adipose tissue. *Methods Enzymol* 2014; **537**: 93–122.

Supplementary Information accompanies this paper on Cell Death and Differentiation website (http://www.nature.com/cdd)